Shear viscosity in two-dimensional dipole systems

N. E. Djienbekov [ORCID], N. Kh. Bastykova, A. M. Bekbussyn [ORCID], T. S. Ramazanov, and S. K. Kodanova [ORCID][*]

Institute for Experimental and Theoretical Physics, Al-Farabi Kazakh National University, 71 Al-Farabi Avenue, 050040 Almaty, Kazakhstan

The results of modeling shear flows in classical two-dimensional (2D) dipole systems are presented. We used the method of nonequilibrium molecular dynamics to calculate the viscosity at various shear rates. The coefficients of shear viscosity are given in the limit of low shear rates for various regimes of interparticle correlation from a weakly correlated gaseous state to a strongly nonideal liquid state near the crystallization point. The calculations were carried out for bare (unscreened) dipole systems, as well as for dipole systems in a polarizable medium that provide screening of the dipole-dipole interaction. The effect of shear thinning in 2D dipole systems is reported for low values of the coupling parameter. In addition, it is shown that dipole systems can become both less and more viscous due to the presence of a screening medium, depending on the degree of interparticle correlation. The optimal simulation parameters are discussed within the framework of the method of nonequilibrium molecular dynamics for determining the shear viscosity of two-dimensional dipole systems. Moreover, we present a simple fitting curve which provides a universal scaling law for both bare dipole-dipole interaction and screened dipole-dipole interaction.

I. INTRODUCTION

Two-dimensional (2D) systems governed by a repulsive dipole-dipole pair interaction are relevant for various systems. For example, the repulsive dipole-dipole interaction is used to describe two-dimensional colloidal systems [1–3]. In complex plasmas, the interaction between charged dust particles can be modified due to external fields and fluxes of ions and electrons [4–11]. It was shown that a repulsive dipole-dipole interaction is realized in complex plasmas under certain conditions [6,9,12–18]. Furthermore, a system of polar molecules [19] and a dipolelike excitonic phase state (created by bound electron-hole excitons) can be described using a model of a classical 2D system of dipoles [20,21].

The aforementioned examples have motivated studies of various properties of classical two-dimensional systems using the repulsive dipole-dipole potential [22]. For example, Khrapak *et al.* [6] investigated thermodynamic and dynamic properties of a classical 2D system of dipoles. Earlier, the characteristic oscillation modes of particles in the 2D dipole system were analyzed by Golden *et al.* [20,21]. In Refs. [20,21], it was demonstrated that a dipolelike excitonic phase state created by bound electron-hole excitons in semiconductors can be described using a model of a classical 2D system of repulsive dipoles. These works on oscillation modes in 2D dipole systems were continued by the study of the dumping of the transverse excitations in the long wavelength domain [23,24]. More recently, Aldakul *et al.* [17] investigated melting, freezing, and the liquid-crystal phase transition point of classical 2D dipole systems. In this work, we extend these studies of 2D dipole systems by modeling shear viscosity and shear flows in classical 2D systems with repulsive dipole interaction across coupling regimes.

In addition to a standard dipole-dipole interaction, in this work we use screened dipole-dipole interaction. In the latter case screening can be due to a polarizable medium surrounding the 2D dipole system [16,17,25]. For example, regarding the aforementioned dipolelike excitonic phase state, it was recently shown that screening due to excess charges modifies electron-hole excitons [26]. In complex plasmas, the stream of ions creates a focused ion cloud near a charged dust particle in the downstream direction due to the attraction of ions by a negative charge of a dust particle and the inelastic collision of ions with atoms [27,28]. The focused ion cloud together with the charged dust particle create a compound particle with zero total charge and a nonzero dipole moment [16]. Additionally, hot electrons—with the electron Debye length being much larger than both the ion Debye length and the size of the compound particle—provide screening of ion and dust particle charges at long distance [16,29]. This leads to the formation of the screened dipole-dipole interaction between compound particles. The impact of screening on the structural properties, oscillation modes, and thermodynamic characteristics of 2D dipole systems was discussed in Ref. [17].

To compute the shear viscosity of 2D systems one can use the reverse nonequilibrium molecular dynamics method (NEMD) [30–32]. This method was used previously to investigate shear flows in classical 2D Yukawa systems [32]. It was shown that the NEMD allows one to determine shear viscosity in good agreement with experimental observation [33]. Moreover, the NEMD allows one to study a non-Newtonian fluid behavior, i.e., when shear viscosity varies with the velocity gradient. One of the peculiar properties of non-Newtonian fluids is the decrease of the viscosity as shear is increased. This effect is referred to as shear thinning. For example, following

---

*kodanova@physics.kz

the original studies on simple liquids by Evans and colleagues [34], such behavior has been reported in dusty plasmas [35]. Additionally, we compare results from the NEMD simulations with the data for the shear viscosity computed using the Green-Kubo relation connecting the shear viscosity and the shear stress autocorrelation function.

This paper is organized as follows: In Sec. II we present the pair interaction potentials. In Sec. III we discuss the computation method and provide simulations details. The results are presented in Sec. IV. This paper is concluded by summarizing the main findings.

II. BARE AND SCREENED DIPOLE-DIPOLE INTERACTIONS

In this work, we present the results of the NEMD simulations for 2D systems with the bare dipole-dipole interaction potential,

$$\beta V(r) = \frac{\Gamma_D}{r^3}, \tag{1}$$

and with the screened dipole-dipole interaction [17,25],

$$\beta V(r) = \frac{\Gamma_D}{r^3}(1 + \kappa r)\exp(-\kappa r), \tag{2}$$

where r is in units of the mean interparticle distance, $\beta = 1/(k_B T)$ is the inverse value of the thermal energy, κ is the screening length, and Γ_D is a parameter characterizing the coupling (correlation) strength [20,21].

The bare repulsive dipole-dipole pair interaction potential (1) has been used to model two-dimensional colloidal systems [1–3] and the dipolelike excitonic phase state of bound electron-hole excitons in semiconductors [20,21]. The screened repulsive dipole-dipole pair interaction (2) provides a description of dipole-dipole interaction in the presence of a highly mobile polarizable background such as electrons in complex plasmas [15,16,25] and an electrolyte screening field of charged colloids [36].

The coupling parameter corresponding to the melting (crystallization) point in the 2D system with bare potential (1) is $\Gamma_m \simeq 67 \pm 4$ [17]. The main effect of screening is to change the pair interaction from a quasi-long-range potential to short-range potential. As a result, the liquid-crystal phase transition point shifts, e.g., to $\Gamma_m \simeq 86 \pm 6$ at $\kappa = 1$ and to $\Gamma_m \simeq 163 \pm 13$ at $\kappa = 2$ [17]. Naturally, we report the shear viscosity results for $\Gamma_D < \Gamma_m$.

III. COMPUTATIONAL METHOD AND SIMULATION DETAILS

A. The NEMD method for generating shear rate

Let us start with a brief description of the essence of the NEMD method for the computation of shear viscosity. The key is to use the definition of shear viscosity in terms of a linear relationship between the momentum flux and velocity gradient [37]:

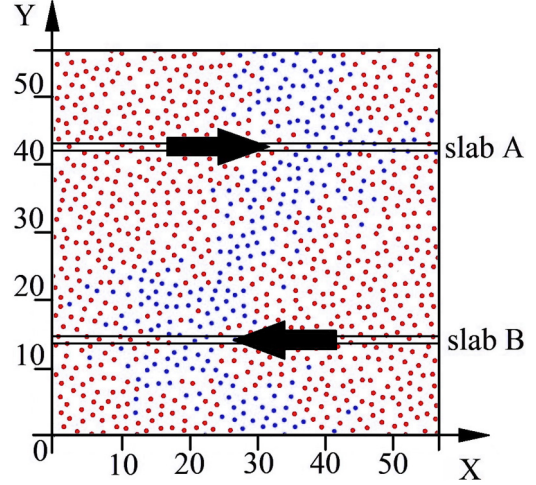$$j_x(p_x) = -\eta \frac{\partial v_x}{\partial y}, \tag{3}$$

FIG. 1. Screenshot from a NEMD simulation after a certain amount of time after the selection of the vertical bar of particles (marked in blue), $\Gamma_D = 30$, $\kappa = 2$. A horizontal shift in the position of the particles can be observed due to the presence of two oppositely directed flows generated in slabs A and B. The length is given in units of the mean interparticle distance (see Sec. III C).

where the momentum flux per unit length j_x, momentum p_x, and shear rate $\partial v_x/\partial y$ are considered to be induced by two oppositely directed streams along the x axis.

In order to calculate shear viscosity, pointlike classical particles in a simulation box with a side length of L are simulated with periodic boundary conditions. In the simulation box, we define two horizontal slabs at the levels $y = L/4$ and $y = 3L/4$ (see Fig. 1). Let us designate these slabs as A and B. From these slabs, according to the NEMD method, the particles with the maximum and minimum values of v_x are identified and simultaneously swapped with a certain frequency (i.e., their momenta are interchanged without changing their coordinates). In other words, the algorithm first selects the fastest particle moving to the right in slab A and the fastest particles moving to the left in slab B and then swaps the velocity values of these particles. As a result, the mean velocity of the particles in slab A is directed in one direction, and that in slab B is directed in the opposite direction. Thus, this exchange of particle velocities conserves energy and mimics two currents flowing in opposite directions. This is illustrated in Fig. 1, where a snapshot from a NEMD simulation is shown.

To find the shear viscosity from Eq. (3), first of all, the dependence of the x component of the mean velocity v_x on the coordinate y is computed. Then, the value of the derivative dv_x/dy in the space between two slabs is calculated using the linear regression method to find the $v_x(y)$ dependence.

Second, the momentum flux is computed using the following relation:

$$j_x(p_x) = \frac{\Delta p}{2Lt}, \tag{4}$$

where the coefficient 2 arises due to the fact that in our case streams pass through two sides of the simulation box, t is the simulation (measurement) time, and Δp is the x component of the total change in momentum as a result of the swapping of velocities of particles during the measurement time.

After finding the values of the shear rate $\partial v_x/\partial y$ and of the momentum flux Δp, shear viscosity is computed as

$$\eta = \frac{\Delta p}{2tLdv_x/dy}. \quad (5)$$

As shown in [30], the shear rate $\partial v_x/\partial y$ depends on the swapping frequency. This means that different slope coefficients will be obtained depending on how often momenta are swapped. On the other hand, the momentum introduced to the system also depends on the swapping frequency. This means that, in general, the shear viscosity of a system can depend on the swapping frequency (i.e., shear rate). However, by varying the momentum exchange frequency parameter, it was found that for sufficiently rare swaps, the viscosity value is independent of the frequency of the momentum exchange within statistical uncertainty [30,32]. It is this value that will be considered physically meaningful and well defined. We note that the NEMD method used in this work is similar to the experimental method employing two counterpropagating laser beams to measure the shear viscosity in dusty plasmas [38], where two oppositely directed flows are generated as illustrated in Fig. 1.

B. Shear viscosity from equilibrium molecular dynamics

As an extra cross-check, we used equilibrium molecular dynamics to calculate the shear viscosity from the Green-Kubo relation connecting the shear viscosity to the shear stress autocorrelation function. We refer to this approach as the equilibrium molecular dynamics method (EMD).

Within the EMD, the Green-Kubo relation for the shear viscosity reads

$$\eta = \frac{1}{Sk_BT}\int_0^\infty C(t)\,dt, \quad C(t) = \langle P^{xy}(t)P^{xy}(0)\rangle, \quad (6)$$

where S is the area of the simulation box and P^{xy} is the off-diagonal element of the pressure tensor,

$$P^{xy} = \sum_{i=1}^N \left[mv_{ix}v_{iy} - \frac{1}{2}\sum_{i\neq j}^N \frac{x_{ij}y_{ij}}{r_{ij}}\frac{\partial V(r_{ij})}{\partial r_{ij}} \right], \quad (7)$$

with N being the number of particles and $r_{ij} = |\mathbf{r}_i - \mathbf{r}_j|$.

In Eq. (6), $C(t)$ is the stress autocorrelation function (SACF) of particles. In practice, in Eq. (6), the upper limit in the integral is limited by the cutoff time, which is defined approximately by the ratio of the simulation box length to the sound speed [39]. Therefore, for a given number of particles, the accuracy of the EMD based calculations depends on the behavior of the SACF at long times. Moreover, for 2D Yukawa systems, the SACF decays slower than t^{-1} and faster than t^{-1} with time for small and large values of the coupling parameter, respectively [39]. The former means a diverging integral in Eq. (6) for low values of the coupling parameter. Nevertheless, it turns out that Eq. (6) with a large enough cutoff time gives meaningful results for the shear viscosity [35,40]. The same is true for the diffusion coefficient computed from the Green-Kubo relation connecting the diffusion coefficient with the velocity autocorrelation function of particles [41].

We use the EMD data to validate the general features related to the dependence of the shear viscosity on the coupling and screening parameters.

C. Simulation parameters

We consider a system of particles enclosed in a square with periodic boundary conditions. Particles with pair interaction potentials (1) and (2) are simulated using molecular dynamics, where streams of particles are introduced as described in the previous section. The side length of the simulation box is defined by the number of particles as $L/a = \sqrt{\pi N}$, with a being the average distance between particles. We consider $N = 1024$ particles. In our simulations, the length is in units of a, and the time is in units of the inverse dipole frequency $1/\omega_d = [p_d^2/(2\pi\epsilon_0 ma^5)]^{-1/2}$ [20,21] (which is introduced in analogy with the plasma frequency but does not describe a real collective oscillation mode), with p_d being the electric dipole moment. The system is characterized by two dimensionless parameters: the first is the coupling parameter Γ_D, and the second is the screening parameter κ. The value of the viscosity is given in units of $\eta_0 = mn\omega_d a^2$. The reduced shear rate is defined as $\gamma^* = (dv_x/dy)(1/\omega_d)$, and velocity values are presented in units of $v_0 = a\omega_d$.

We study the dependence of shear viscosity on the coupling parameter Γ_D considering $\kappa = 0$, $\kappa = 1$, and $\kappa = 2$. The case $\kappa = 0$ corresponds to a bare dipole-dipole interaction with the pair potential (1). For different κ values, a system crystallizes at different Γ_D; therefore, for systems with different inverse screening lengths, the coupling parameter varies within different limits. The results presented in the following sections are measured and averaged over $1000\omega_d^{-1}$. For cross validation of our NEMD code, we have reproduced data for the shear viscosity of a 2D Yukawa system reported by Donkó et al. [33]. The corresponding comparison of our results with those of Donkó et al. is shown in the Appendix.

Using the EMD method, we calculated the shear viscosity for three values of the coupling parameter, $\Gamma_D = 1$, $\Gamma_D = 10$, and $\Gamma_D \approx \Gamma_m$. The coupling parameter values Γ_m corresponding to the melting (crystallization) point for different screening parameters were reported by Aldakul et al. [17]. The number of particles in our EMD simulations was set to $N = 10^4$. The SACF data were averaged over 20 independent simulations. The SACF is presented in units of $C_0 = \eta_0\omega_d k_B T S$.

In the case of the bare dipole-dipole interaction, a direct summation of the interaction force in MD is known to be highly time-consuming and inefficient due to scaling as $O(N^2)$ with respect to the number of particles. To avoid this problem and reduce scaling to $O(N)$, the gradient-shifted force (GSF) electrostatics [42] based on the Wolf method [43] is used. Within the GSF electrostatics, we set the cutoff value and dumping coefficient to $r_c/a = 12a$ and $\alpha = 0.2a^{-1}$, respectively. These values allow us to find converged data for structural and dynamical properties of 2D dipole systems [17].

IV. RESULTS

A. Shear thinning effect

To begin with, in Fig. 2 we show the velocity distribution of particles along the y axis, i.e., perpendicular to the direction of
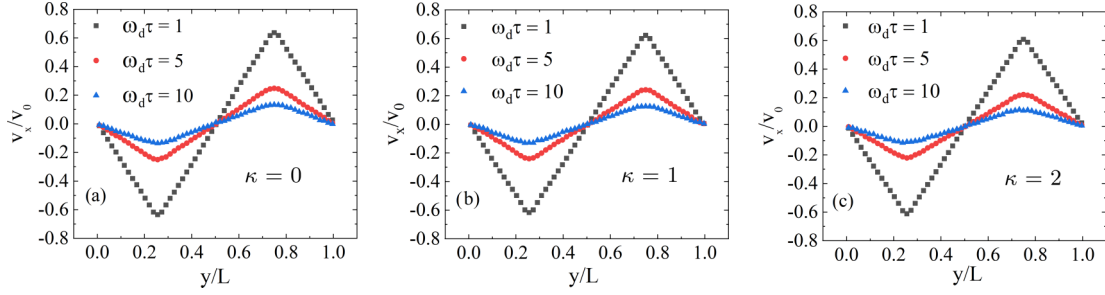
FIG. 2. Velocity profiles perpendicular to the direction of flows at $\Gamma_D = 1$ for (a) $\kappa = 0$, (b) $\kappa = 1$, and (c) $\kappa = 2$. The results are presented for different values of the period of momenta exchange between flows.

flows, at different values of the period of momentum swap τ between slabs A and B. The results presented in Figs. 2(a)–2(c) are for a weakly correlated system with $\Gamma_D = 1$ and with $\kappa = 0$, $\kappa = 1$, and $\kappa = 2$, respectively. The presented data are for the momenta exchange period $\omega_d\tau = 1$, 5, and 10. From Fig. 2 we clearly observe that the more frequently the permutation of moments occurs, the greater the shear rate $\partial v_x/\partial y$ is. Further, as expected, the distribution of velocities between slabs A and B is a linear function of the distance between these slabs.

In Fig. 3, we present the velocity distribution of particles in the case of the strongly correlated system with $\Gamma_D = 30$. As in the weakly correlated case, we observe an increase in the shear rate with a decrease in the period of momentum exchange in the slabs. Furthermore, the velocity distribution between streams remains a linear function of the distance. This behavior is general up to a crystallization point and allows us to compute shear viscosity in a wide range of coupling parameter values using the NEMD method.

The results presented in Figs. 2 and 3 were measured after the system reached the stationary (equilibrium) regime. The change in time of the shear rate γ at $\tau\omega_d = 10$ is presented in Figs. 4(a) and 4(b) for $\Gamma_D = 1$ and $\Gamma_D = 30$, respectively. From Figs. 4(a) and 4(b), we observe that to obtain a physically valid viscosity, one needs to model for a long enough time that the angle of inclination becomes approximately constant. For example, at a momentum exchange period of $10\,\omega_d^{-1}$, it took about $60\,000\,\omega_d^{-1}$ for the bare dipole system and about $45\,000\,\omega_d^{-1}$ for the screened dipole system to reach a stationary regime. Therefore, a system with a stronger interparticle correlation takes longer to reach a steady state. In Fig. 4(c), the dependence of the shear rate on the momentum

exchange period τ is shown. As expected, one can observe an increase in the shear rate with a decrease in the period of momentum exchange in the slabs.

To obtain a physically correct shear viscosity, i.e., one which is independent of shear rate, it is necessary to permute the momentum as rarely as possible. For the considered parameters, the optimal value of the frequency of momentum exchange is found to be once every $10\omega_d^{-1}$ time period. If one increases the frequency of the momentum exchange, then shear viscosity can become a function of shear rate. In Fig. 5, the shear viscosity at different values of the momentum permutation period is presented for $\Gamma_D = 1$ and $\Gamma_D = 30$. From Fig. 5, we clearly see that at $\Gamma_D = 1$ (independent of screening parameter), the shear viscosity is approximately independent of the momentum exchange period at $\tau\omega_d \gtrsim 10$. In contrast, at $\Gamma_D = 1$ and $\tau\omega_d < 10$, we observe that the shear viscosity decreases as the momentum permutation period decreases.

Figure 6 shows the dependence of the viscosity on the shear rate at $\Gamma_D = 1$ and $\Gamma_D = 30$. From Fig. 6, one can observe that the viscosity value approaches an equilibrium value with the decrease in the shear rate. For $\Gamma_D = 30$, the change in the momentum permutation period in the range $10^{-1} \leqslant \tau\omega_d \leqslant 20$ does not lead to a large enough change in the shear rate. As a result, we do not observe a strong impact of the shear rate variation on the viscosity value at $\Gamma_D = 30$.

The decrease in the momentum permutation period is equivalent to the increase in the shear rate, as demonstrated in Figs. 2 and 3. The effect of the reduction of the shear viscosity with the increase in the shear rate is called the shear thinning effect. Thus, we are able to observe from Figs. 5 and 6 the effect of shear thinning in a two-dimensional system of particles interacting through the repulsive dipole potential
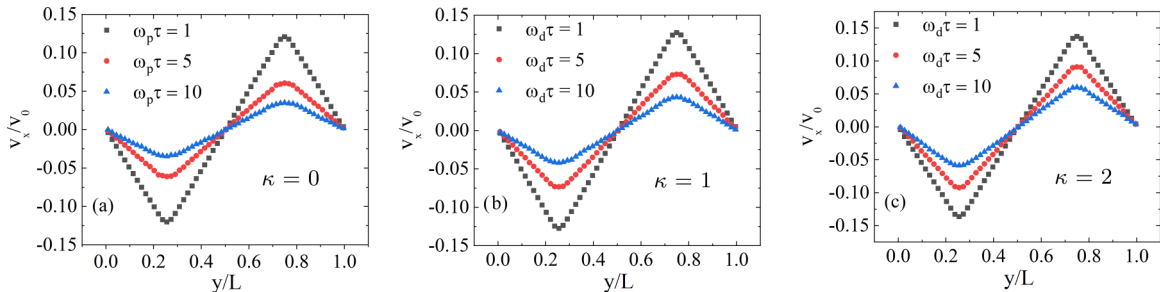

FIG. 3. Velocity profiles perpendicular to the direction of flows at $\Gamma_D = 30$ for (a) $\kappa = 0$, (b) $\kappa = 1$, and (c) $\kappa = 2$. The results are presented for different values of the period of momenta exchange between flows.
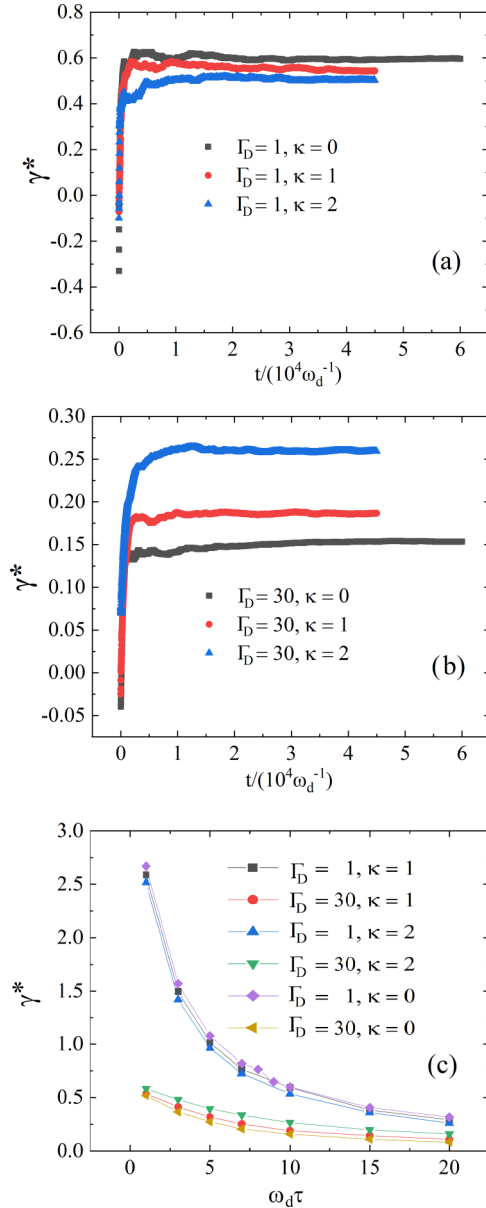
FIG. 4. The dependence of the shear rate on time for different parameters: (a) $\Gamma_D = 1$; $\kappa = 0, 1, 2$; $\omega_d\tau = 10$. (b) $\Gamma_D = 30$; $\kappa = 0, 1, 2$; $\omega_d\tau = 10$. (c) The dependence of the shear rate on the period of momentum exchange in the slabs.

in the weakly correlated regime (e.g., at $\Gamma_D = 1$). One can expect to observe the shear thinning effect at $\Gamma_D = 30$ in the case $\tau\omega_d \ll 10^{-1}$, but it seems to be a rather unrealistic limit in which the particles dynamics is strongly disturbed at the length scale of the mean interparticle distance. Therefore, next, we focus on physically meaningful results for the shear viscosity values in the limit of low shear rates.

B. Shear viscosity

Let us consider shear viscosity in the limit of low shear rates in more detail. For the screening parameters considered in this work, the phase transition point lies in the intervals $\Gamma_m = 67 \pm 4$ at $\kappa = 0$ and $\Gamma_m = 86 \pm 6$ at $\kappa = 1$ and in
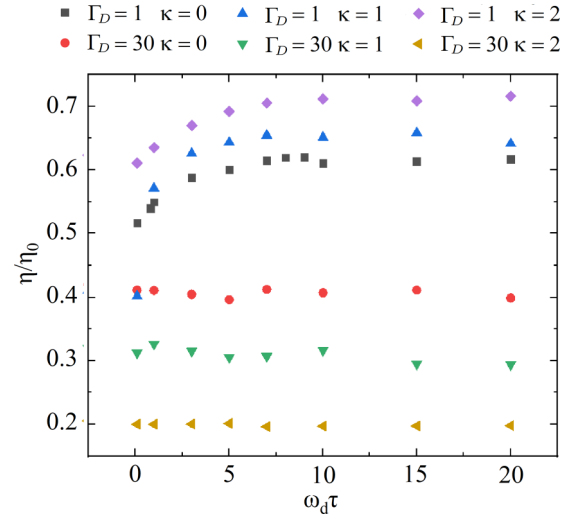

FIG. 5. Shear viscosity as a function of the momentum exchange frequency for selected values of the coupling parameter Γ_D.

the range $\Gamma_m = 163 \pm 13$ at $\kappa = 2$. We varied the coupling parameter of the system from $\Gamma_D = 1$ to approximately $\Gamma_D = \Gamma_m$.

From Fig. 7 we see that the shear viscosity has a nonmonotonic dependence on the coupling parameter with a minimum at a moderate coupling value. More specifically, the minimum of the shear viscosity occurs at $\Gamma_{min} \approx 10$ for the system with $\kappa = 0$, at $10 \leqslant \Gamma_{min} < 20$ for the system with $\kappa = 1$, and at $\Gamma_{min} \approx 30$ for the screened dipole system with $\kappa = 2$. The change in the coupling parameter to lower or larger values results in the increase in the shear viscosity. This behavior is similar to that observed for Yukawa systems and explained to be the result of the competition between the kinetic and correlation parts of the pressure tensor [44].

Additionally, from Fig. 7 we can observe that the minimum value of the shear viscosity decreases with the increase in the screening parameter. Furthermore, shear viscosity values at $\kappa = 0$, $\kappa = 1$, and $\kappa = 2$ are approximately the same at $\Gamma_D = 5$. At $\Gamma_D < 5$, screening leads to an increase in shear
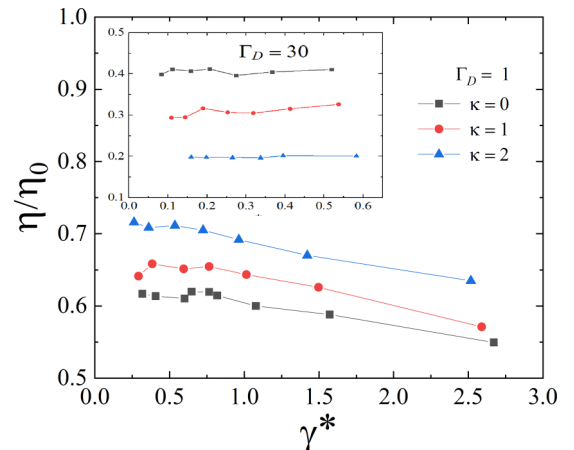

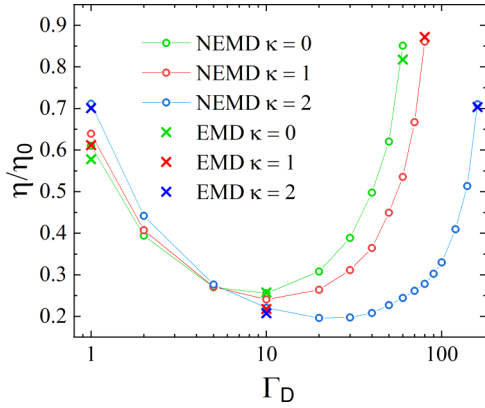FIG. 6. Shear viscosity as a function of the shear rate for selected values of the coupling parameter Γ_D.

FIG. 7. Shear viscosity in the limit of low shear rates from the NEMD and EMD simulations.

viscosity. In contrast, at $\Gamma_D > 5$, screening leads to a decrease in shear viscosity.

As a sanity test of the NEMD results for 2D dipole systems, we performed calculations using equilibrium MD data and the Green-Kubo relation (6). In Figs. 8(a)–8(c), we present results for the SACF at $\kappa = 0$, $\kappa = 1$, and $\kappa = 2$, respectively, for $\Gamma_D = 1$, $\Gamma_D = 10$, and $\Gamma_D \approx \Gamma_m$. Γ_m is the coupling parameter corresponding to the melting (crystallization) point from Ref. [17]. The general behavior of the SACF is a decay with the increase in time. However, at $t > 10\omega_d^{-1}$, the SACF becomes strongly affected by noise due to the finite number of particles in the main cell. Here we used $N = 10^4$ particles and averaged over 20 independent simulations. For an accurate analysis of the behavior of the SACF at long times, we need many more particles in the main cell [39]. We do not explore this aspect of the SACF here, but we use the computed SACF results to see whether the NEMD data are adequate.

From Fig. 7, we see that the EMD results computed using the SACF are in good agreement with the NEMD data with a disagreement of about 4% at $\Gamma_D = 1$ for $\kappa = 0$ and $\kappa = 1$. The largest disagreement of 8% is observed for $\Gamma_D = 10$ and $\kappa = 1$. In the other considered cases, the discrepancy between the NEMD and EMD data does not exceed a few percent. These deviations are expected since the utility of the Green-Kubo relation for the viscosity calculations of 2D systems is problematic, as discussed in Sec. III B. Nevertheless, from Fig. 8, we see that the EMD data behave similarly to the NEMD data with respect to the dependence on the coupling and screening parameters.

The values of the shear viscosity computed using the NEMD method are given in Table I. Additionally, for comparison, the shear viscosity results calculated from the EMD method are shown in Table II.

C. Universal scaling law

It is known that one can express the viscosity dependence on temperature via some universal scaling law [45]. For example, in the case of 2D Yukawa systems, one can find such an expression by expressing the viscosity value in units of $\eta_E = mn\omega_E a^2$ and as a function of the reduced temperature $T^* = T/T_m$, where ω_E is the Einstein frequency and T_m is a melting temperature.
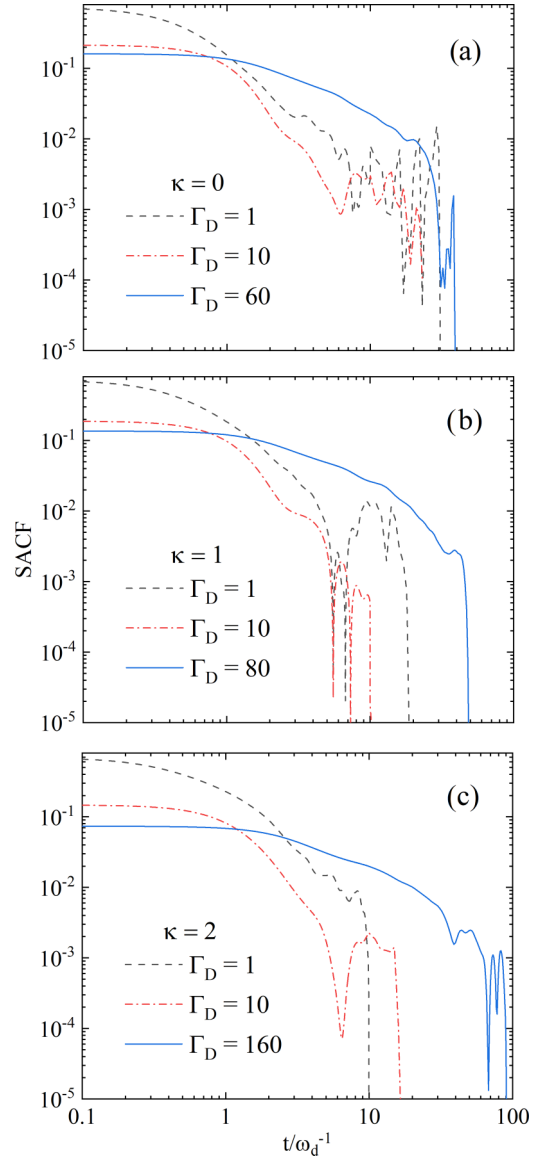

FIG. 8. The SACF results for $\Gamma_D = 1$, $\Gamma_D = 10$, and $\Gamma_D \approx \Gamma_m$ at (a) $\kappa = 0$, (b) $\kappa = 1$, and (c) $\kappa = 2$.

We have performed an analysis of the computed viscosity data using η_E. For that, the Einstein frequency values at different parameters were calculated as [46]

$$\omega_E^2 = \frac{1}{3m} \sum_{i \neq j} \Delta V(\mathbf{r_i} - \mathbf{r_j}). \tag{8}$$

The η/η_E dependence on T/T_m is presented in Fig. 9 for $\kappa = 0$, $\kappa = 1$, and $\kappa = 2$. From Fig. 9, one can clearly see that there is some universality in the dependence of η/η_E on T/T_m, which is not sensitive to the screening parameter.

In the case of 2D Yukawa systems, the universal scaling law for $\eta/\eta_E(T/T_m)$ reads [32]

$$\eta/\eta_E = a_1 T^* + b_1 T^{*-1} + c_1, \tag{9}$$

where a_1, b_1, and c_1 are fitting parameters and $T^* = T/T_m$ is the reduced temperature.

TABLE I. The shear viscosity values in the limit of low shear rates for dipole systems with $\kappa = 0$, $\kappa = 1$, and $\kappa = 2$, obtained with the NEMD method as described in Sec. III A.

Γ_D	$\kappa = 0$	$\kappa = 1$	$\kappa = 2$
1	0.61	0.64	0.71
2	0.39	0.41	0.44
5	0.27	0.27	0.28
10	0.26	0.24	0.22
20	0.31	0.26	0.20
30	0.39	0.31	0.20
40	0.50	0.36	0.21
50	0.62	0.45	0.23
60	0.85	0.54	0.24
70		0.67	0.26
80		0.86	0.28
90			0.30
100			0.33
120			0.41
140			0.51
160			0.71

First, we checked whether Eq. (9) can describe 2D dipole systems. The best fit obtained using Eq. (9) and the method of least squares is shown in Fig. 9 by the dashed line, where $a_1 = 0.00187897$, $b_1 = 0.9$, and $c_1 = 0.19964258$. Clearly, Eq. (9) is not able to provide an adequate universal scaling law. Instead, we found that a much better description is provided by replacing the T^{*-1} term with T^{*-2}, i.e., by using

$$\eta/\eta_E = a_2 T^* + b_2 T^{*-2} + c_2, \tag{10}$$

where a_2, b_2, and c_2 are fitting parameters.

The best fit based on Eq. (10) is shown in Fig. 9 by the solid line, where $a_2 = 0.00124$, $b_2 = 1.16076$, and $c_2 = 0.27754$. From Fig. 9, we observe that Eq. (10) provides an adequate universal scaling law for 2D repulsive dipole systems.

V. CONCLUSION

The shear viscosity of two-dimensional dipole and screened dipole systems was investigated using the NEMD. The optimal values of the momentum exchange frequency and equilibration time were analyzed to compute the shear viscosity values for different coupling and screening parameters. The dependence of the shear viscosity on the coupling parameter Γ in the limit of low shear rates for different screening parameters was presented. It was found that screening leads

TABLE II. The shear viscosity values for dipole systems with $\kappa = 0$, $\kappa = 1$, and $\kappa = 2$, obtained with the EMD method as described in Sec. III B.

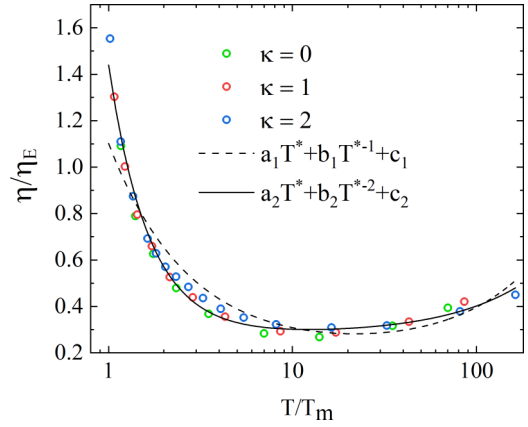| Γ_D	$\kappa = 0$	$\kappa = 1$	$\kappa = 2$
1	0.58	0.61	0.70
10	0.26	0.22	0.21
60	0.82		
80		0.87	
160			0.70

FIG. 9. The dependence of the shear viscosity on the reduced temperature T/T_m, where the shear viscosity is presented in units of η_E. The dashed line is the best fit obtained using Eq. (9); the solid line is the best fit based on Eq. (10). The data were fitted using the method of least squares.

to an increase in the shear viscosity at $\Gamma_D < 5$. In contrast, at $\Gamma_D > 5$ the shear viscosity of 2D dipole systems decreases with an increasing screening parameter. As expected, the shear viscosity of 2D dipole systems has a minimum at intermediate coupling parameters. The value of the coupling parameter corresponding to the minimum of the shear viscosity shifts to larger values with an increase in the screening degree. Furthermore, a shear thinning effect was revealed for 2D dipole systems for low values of the coupling parameter.

Our extensive NEMD simulations have allowed us to calculate the shear viscosity of classical 2D repulsive dipole systems. Furthermore, we found a simple fitting curve which provides a single universal scaling law valid for both the bare dipole-dipole pair interaction potential and the screened dipole-dipole pair interaction potential. Taking into account the relevance of dipole systems for various fields of physics and the general interest from the point of view of statistical physics, we believe that the present study is a valuable addition to the physics of strongly correlated 2D systems.
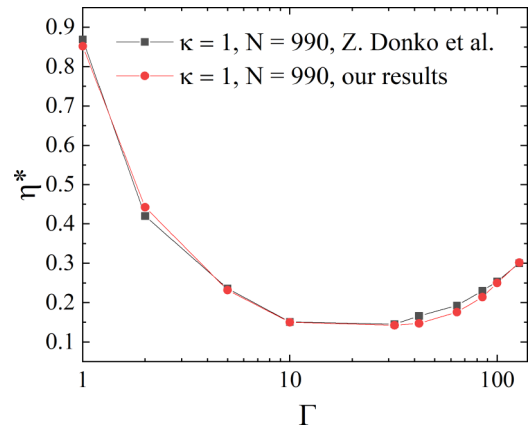

FIG. 10. Shear viscosity in the limit of low shear rates for the 2D Yukawa system. A comparison with the data from Ref. [32] is presented.

APPENDIX: THE SHEAR VISCOSITY OF CLASSICAL 2D YUKAWA SYSTEMS

In order to verify the correctness of our implementation of the NEMD method, we computed the shear viscosity of 2D Yukawa systems in the limit of low shear rates and validated our results by a comparison with previously published data by Donkó *et al.* [32].

In the case of the Yukawa system, the pair interaction potential is defined as $U = Q^2 \exp(-r/\lambda_D)/4\pi\varepsilon_0 r$. The Yukawa system is characterized by the following dimensionless parameters: $\Gamma = Q^2/2\pi\varepsilon_0 a k_B T$, $\kappa = a/\lambda_D$, and $a = (1/\pi n)^{1/2}$, where a is the Wigner-Seitz radius, λ_D is the Debye screening length, n is the number density of particles, $\omega_p = (Q^2/2\pi\varepsilon_0 m a^3)^{1/2}$, ω_p is the 2D analog of the plasma frequency, and $\eta^* = \eta/mn\omega_p a^2$.

The comparison of our results with the data from Ref. [32] is presented in Fig. 10 for $\kappa = 1$. As can be seen from Fig. 10, our results have a fairly accurate agreement with the data from Ref. [32].

[1] J. Zanghellini, P. Keim, and H. H. von Grünberg, The softening of two-dimensional colloidal crystals, J. Phys.: Condens. Matter **17**, S3579 (2005).

[2] H. H. von Grünberg, P. Keim, K. Zahn, and G. Maret, Elastic Behavior of a Two-Dimensional Crystal Near Melting, Phys. Rev. Lett. **93**, 255703 (2004).

[3] E. Pretti, H. Zerze, M. Song, Y. Ding, R. Mao, and J. Mittal, Size-dependent thermodynamic structural selection in colloidal crystallization, Sci. Adv. **5**, eaaw5912 (2019).

[4] R. Kompaneets, G. E. Morfill, and A. V. Ivlev, Design of new binary interaction classes in complex plasmas, Phys. Plasmas **16**, 043705 (2009).

[5] R. Kompaneets, G. E. Morfill, and A. V. Ivlev, Interparticle Attraction in 2D Complex Plasmas, Phys. Rev. Lett. **116**, 125001 (2016).

[6] S. A. Khrapak, N. P. Kryuchkov, and S. O. Yurchenko, Thermodynamics and dynamics of two-dimensional systems with dipolelike repulsive interactions, Phys. Rev. E **97**, 022616 (2018).

[7] Z. A. Moldabekov, Y. K. Aldakul, N. K. Bastykova, S. Sundar, and A. Cangi, Higher harmonics in complex plasmas with alternating screening, Phys. Rev. Res. **3**, 043187 (2021).

[8] Z. A. Moldabekov, P. Ludwig, J.-P. Joost, M. Bonitz, and T. S. Ramazanov, Dynamical screening and wake effects in classical, quantum, and ultrarelativistic plasmas, Contrib. Plasma Phys. **55**, 186 (2015).

[9] S. K. Kodanova, T. S. Ramazanov, N. K. Bastykova, and Z. A. Moldabekov, Effect of dust particle polarization on scattering processes in complex plasmas, Phys. Plasmas **22**, 063703 (2015).

[10] S. Sundar and Z. A. Moldabekov, Oblique magnetic field influence on the wakefield in complex plasmas, Plasma Phys. Controlled Fusion **62**, 105018 (2020).

[11] S. Sundar and Z. A. Moldabekov, Ultracold ions wake in dusty plasmas, New J. Phys. **22**, 033028 (2020).

[12] G. Cooper, Shielding of slow test particles in a plasma, Phys. Fluids **12**, 2707 (1969).

[13] R. Kompaneets, G. E. Morfill, and A. V. Ivlev, Wakes in complex plasmas: A self-consistent kinetic theory, Phys. Rev. E **93**, 063201 (2016).

[14] G. I. Sukhinin and A. V. Fedoseev, Formation of a trapped-ion cloud around a dust particle in low-density plasma, IEEE Trans. Plasma Sci. **38**, 2345 (2010).

[15] G. Lapenta, Dipole Moments on Dust Particles Immersed in Anisotropic Plasmas, Phys. Rev. Lett. **75**, 4409 (1995).

[16] G. Sukhinin, M. Salnikov, A. Fedoseev, and A. Rostom, Plasma polarization and wake formation behind a dust particle in an external electric field, IEEE Trans. Plasma Sci. **46**, 749 (2018).

[17] Y. K. Aldakul, Z. A. Moldabekov, and T. S. Ramazanov, Melting, freezing, and dynamics of two-dimensional dipole systems in screening bulk media, Phys. Rev. E **102**, 033205 (2020).

[18] T. S. Ramazanov, A. Z. Gabdulin, and Z. A. Moldabekov, MD simulation of charged dust particles with dipole moments, IEEE Trans. Plasma Sci. **43**, 4187 (2015).

[19] M. Lemeshko, R. V. Krems, J. M. Doyle, and S. Kais, Manipulation of molecules with electromagnetic fields, Mol. Phys. **111**, 1648 (2013).

[20] K. I. Golden, G. J. Kalman, P. Hartmann, and Z. Donkó, Dynamics of two-dimensional dipole systems, Phys. Rev. E **82**, 036402 (2010).

[21] K. I. Golden, G. J. Kalman, Z. Donko, and P. Hartmann, Acoustic dispersion in a two-dimensional dipole system, Phys. Rev. B **78**, 045304 (2008).

[22] S. A. Khrapak, Lindemann melting criterion in two dimensions, Phys. Rev. Res. **2**, 012040(R) (2020).

[23] L. A. Mistryukova, N. P. Kryuchkov, S. A. Khrapak, I. S. Golyak, and S. O. Yurchenko, Collective excitations in two-dimensional fluid with dipole-like repulsive interactions, Journal of Physics: Conference Series **1348**, 012097 (2019).

[24] N. P. Kryuchkov, L. A. Mistryukova, A. V. Sapelkin, V. V. Brazhkin, and S. O. Yurchenko, Universal Effect of Excitation Dispersion on the Heat Capacity and Gapped States in Fluids, Phys. Rev. Lett. **125**, 125501 (2020).

[25] T. S. Ramazanov, Z. A. Moldabekov, and M. T. Gabdullin, Multipole expansion in plasmas: Effective interaction potentials between compound particles, Phys. Rev. E **93**, 053204 (2016).

[26] A. Tiene, J. Levinsen, M. M. Parish, A. H. MacDonald, J. Keeling, and F. M. Marchetti, Extremely imbalanced two-dimensional electron-hole-photon systems, Phys. Rev. Res. **2**, 023089 (2020).

[27] G. I. Sukhinin, A. V. Fedoseev, M. V. Salnikov, A. Rostom, M. M. Vasiliev, and O. F. Petrov, Plasma anisotropy around a dust particle placed in an external electric field, Phys. Rev. E **95**, 063207 (2017).

[28] G. I. Sukhinin, A. V. Fedoseev, S. N. Antipov, O. F. Petrov, and V. E. Fortov, Effect of trapped ions and nonequilibrium

electron-energy distribution function on dust-particle charging in gas discharges, Phys. Rev. E **79**, 036404 (2009).

[29] Z. A. Moldabekov, P. Ludwig, J.-P. Joost, M. Bonitz, and T. S. Ramazanov, Wakefields in streaming plasmas: Characteristics of the induced charge density distribution, arXiv:1709.09531 (2017).

[30] F. Müller-Plathe, Reversing the perturbation in nonequilibrium molecular dynamics: An easy way to calculate the shear viscosity of fluids, Phys. Rev. E **59**, 4894 (1999).

[31] K. Y. Sanbonmatsu and M. S. Murillo, Shear Viscosity of Strongly Coupled Yukawa Systems on Finite Length Scales, Phys. Rev. Lett. **86**, 1215 (2001).

[32] Z. Donkó, J. Goree, P. Hartmann, and K. Kutasi, Shear Viscosity and Shear Thinning in Two-Dimensional Yukawa Liquids, Phys. Rev. Lett. **96**, 145003 (2006).

[33] Z. Donkó, P. Hartmann, and J. Goree, Shear viscosity of strongly-coupled two-dimensional Yukawa liquids: Experiment and modeling, Mod. Phys. Lett. B **21**, 1357 (2007).

[34] B. L. Holian and D. J. Evans, Shear viscosities away from the melting line: A comparison of equilibrium and nonequilibrium molecular dynamics, J. Chem. Phys. **78**, 5147 (1983).

[35] B. Liu and J. Goree, Shear Viscosity of Two-Dimensional Yukawa Systems in the Liquid State, Phys. Rev. Lett. **94**, 185002 (2005).

[36] J. C. Everts, B. Senyuk, H. Mundoor, M. Ravnik, and I. I. Smalyukh, Anisotropic electrostatic screening of charged colloids in nematic solvents, Sci. Adv. **7**, eabd0662 (2021).

[37] P. W. Atkins and I. R. McDonald, *Physical Chemistry*, 5th ed. (Oxford University Press, Oxford, 1994).

[38] V. Nosenko and J. Goree, Shear Flows and Shear Viscosity in a Two-Dimensional Yukawa System (Dusty Plasma), Phys. Rev. Lett. **93**, 155004 (2004).

[39] Z. Donkó, J. Goree, P. Hartmann, and B. Liu, Time-correlation functions and transport coefficients of two-dimensional Yukawa liquids, Phys. Rev. E **79**, 026401 (2009).

[40] Y. Feng, J. Goree, B. Liu, and E. G. D. Cohen, Green-Kubo relation for viscosity tested using experimental data for a two-dimensional dusty plasma, Phys. Rev. E **84**, 046412 (2011).

[41] P. Hartmann, J. C. Reyes, E. G. Kostadinova, L. S. Matthews, T. W. Hyde, R. U. Masheyeva, K. N. Dzhumagulova, T. S. Ramazanov, T. Ott, H. Kählert, M. Bonitz, I. Korolov, and Z. Donkó, Self-diffusion in two-dimensional quasimagnetized rotating dusty plasmas, Phys. Rev. E **99**, 013203 (2019).

[42] M. Lamichhane, J. D. Gezelter, and K. E. Newman, Real space electrostatics for multipoles. I. Development of methods, J. Chem. Phys. **141**, 134109 (2014).

[43] D. Wolf, P. Keblinski, S. R. Phillpot, and J. Eggebrecht, Exact method for the simulation of Coulombic systems by spherically truncated, pairwise r-1 summation, J. Chem. Phys. **110**, 8254 (1999).

[44] Z. Donkó and P. Hartmann, Shear viscosity of strongly coupled Yukawa liquids, Phys. Rev. E **78**, 026408 (2008).

[45] D. Huang, S. Lu, M. S. Murillo, and Y. Feng, Origin of viscosity at individual particle level in Yukawa liquids, Phys. Rev. Res. **4**, 033064 (2022).

[46] T. Saigo and S. Hamaguchi, Shear viscosity of strongly coupled Yukawa systems, Phys. Plasmas **9**, 1210 (2002).